Computer Aided Design of New Forging Technology for Crank Shafts

W. Walczyk[1)], A. Milenin[2)]*, and M. Pietrzyk[2)]

[1)] Metal Forming Institute, Jana Pawła II nr 14, 61-139, Poznań, Poland
[2)] Akademia Górniczo-Hutnicza, Mickiewicza 30, 30-059 Kraków, Poland
* Corresponding author; e-mail: milenin@agh.edu.pl

Application of numerical simulations to improve forging technology for crank shafts is the objective of this work. Plastometric tests were performed for steels used for manufacturing of crank shafts and a rheological model for these steels was determined. Inverse analysis was applied for the identification of the model parameters. This model was implemented in the finite element software and simulations of various variants of forging were performed. Results of simulations were used to select the best variant, which gives the lowest loses of the material and proper shape of the final product.

Keywords: finite element method, forging of crank shafts, inverse analysis

Submitted on 22 May 2010, accepted on 12 August 2010

Introduction

The technology of forging of crank shafts developed at the Metal Forming Institute in Poznan, Poland (TR method – following the name of the inventor) [1, 2] is the subject of this paper. This technology gives very good results when shape of the shoulders of the crank is close to an ellipse. New constructions of crank shafts require large juts at the side of journals of main bearings. In consequence, machining of deep grooves in the stock material is needed. It is technologically inconvenient and it leads to an increase of material waste, what causes an increase of the costs of machining. To avoid this inconvenience, additional forging operation is introduced. This is an unsymmetrical preupsetting of the stock material, which involves proper flow of the material needed to obtain required shape of the crank shoulders. There are several possible variants of his process and experimental analysis of all variants would be very costly. Thus, the objective of the present work is the development of a finite element model of forging of crankshafts and the application of this model to simulate various technological variants.

TR process

Idea of the conventional TR process is shown in **Figure 1**. In Figure 1a, a part of the stock material is seen in the tools, which are in the idle positions at the start of a cycle. In Figure 1b, the forming cycle is completed and the set of tools is fully closed. A crank throw of a crank shaft has been formed; the bending tool (3) and the anvil (5) shape the pin portion, and the crank webs are formed by upsetting caused by horizontal movement of the face die inserts (1_1; 2_1). The modification of this process based on simulations is the subject of the present work.

Models

Rheological model. Two steels with chemical composition given in **Table 1** are used for forging of crank shafts. Axisymmetrical compression tests were carried out on the Gleeble 3800 simulator at the Institute for Ferrous Metallurgy in Gliwice, Poland to determine rheological models for these steels. Sample dimensions were $\phi 12 \times 10$ mm. The tests were performed at temperatures of 1000, 1100 and 1200 °C and at strain rates of 0.1, 0.5, 1 and 10 s^{-1}, which cover the conditions of forging of crank shafts.

Due to various disturbances (effect of friction, deformation heating etc), the direct interpretation of results may cause errors. It is shown in a number of publications [3–5]

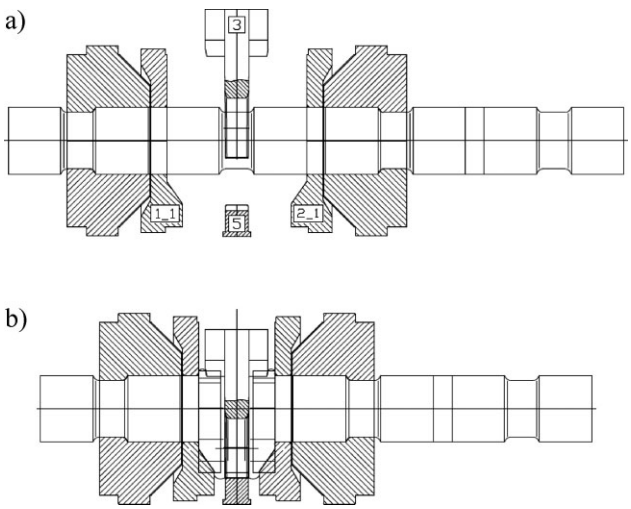

Figure 1. Schematic illustration of the conventional TR process: a – start of a cycle, b – forming cycle is completed.

Table 1. Chemical compositions of the investigated steels, wght%.

Steel	C	Mn	Si	Cr	Cu	Ni	Mo	V	Co	Nb
30CrMo12	0.40	0.42	0.28	2.9	0.068	0.081	0.37	0.084	0.044	0.027
34CrNiMo6	0.40	0.61	0.19	1.6	0.084	1.6	0.20	0.13	0.066	0.040

that application of the inverse analysis for the interpretation of plastometric tests minimizes the influence of these disturbances and allows flow stress to be determined independent of the method of testing. Friction factor has to be known to determine the flow stress, therefore, this factor evaluated for the Gleeble simulator in [6] and equal to 0.12 is used in the present project.

The inverse algorithm described in [4] was used. This algorithm is described briefly below. The flow stress model is identified by searching for the minimum of the objective function, which is defined as a square root error between measured and calculated loads:

$$\Phi = \sqrt{\frac{1}{Npt}\sum_{i=1}^{Npt}\left[\frac{1}{Nps}\sum_{j=1}^{Nps}\left(\frac{F_{cji}(\mathbf{x},\mathbf{p}_i)-F_{mji}}{F_{mji}}\right)^2\right]} \qquad (1)$$

where: F_{mij}, F_{cij} – measured and calculated loads, Npt – number of tests, Nps – number of load measurements in one test, $\mathbf{p}$ – vector of process parameters (strain rates, temperatures), $\mathbf{x}$ – vector of coefficients in the models (rheological parameters, friction coefficient).

The direct problem model is based on the finite element program described in [7, 8] and is defined as simulation of the axisymmetrical compression tests. The finite element code used for the calculations is based on the rigid-plastic approach coupled with the solution of the heat transport equation. Detailed description of this model is given in [7] and it is not repeated here.

Selected results of the experiments are presented in **Figure 2**. It can be seen that differences between the two steels are negligible. Only slightly larger loads were obtained for the 30CrMo12 steel, in particular at low stain rates. The rheological models were determined for both steels separately, although the differences in simulation of forging process are not expected. Therefore, all results of simulations are presented for one steel only.

The inverse analysis of rheological law was performed in 2 steps, as shown in [3]. The flow stress as a function of strain given in a tabular form for each test separately was determined

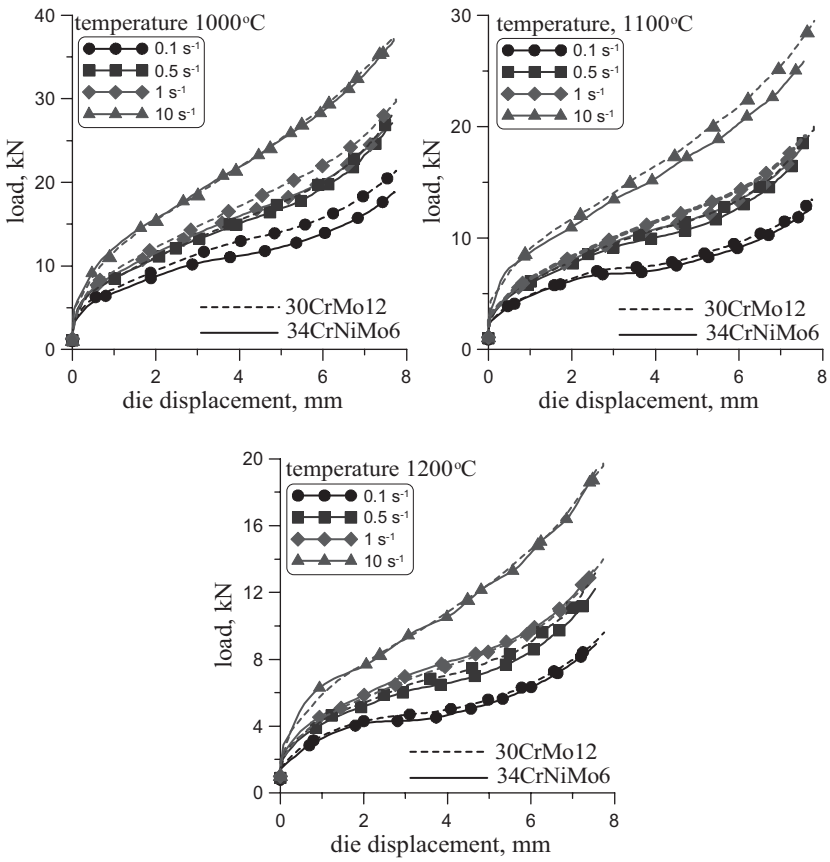

Figure 2. Loads recorded during the tests for the 30CrMo12 (dotted lines) and 34CrNiMo6 (solid lines) steels.

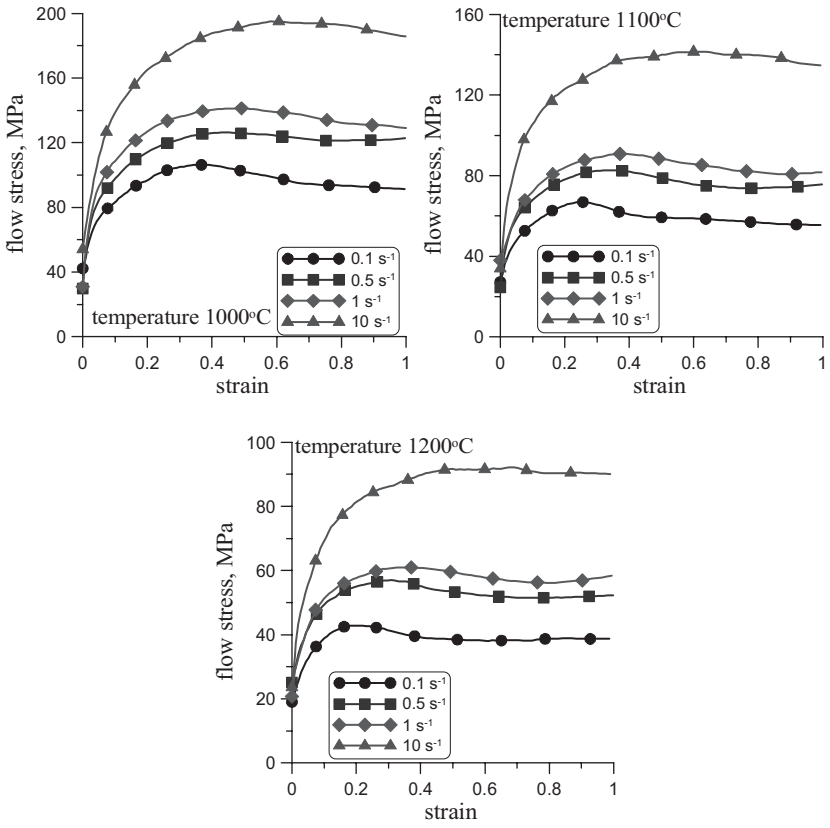

Figure 3. Flow stress determined in the first step of the inverse analysis as function of strain for the 30CrMo12 steel.

first and the results are presented in **Figure 3**. This flow stress, when implemented into the finite element code, give perfect agreement between the measured and predicted loads during the tests.

Identification of coefficients in the flow stress model was the objective of the second part of the inverse analysis. These coefficients were the variables in the objective function (1), which is defined as a square root error between measured and predicted loads in all tests performed for the investigated steels. It is expected that when the flow stress function is introduced in the FE code, the agreement between measured and predicted loads may not be as perfect as in the case of the stress-strain relation introduced in a tabular form. The agreement in this case depends on the function's capability of reproducing properly behaviour of the deformed material, which is not always easy. Several functions were tested within the project and the two of them were selected. The first is Hansel and Spittel equation [9]:

$$\sigma = A\varepsilon^{n}\exp(-B\varepsilon)\dot{\varepsilon}^{m}\exp(-CT) \tag{2}$$

The second considered model is a modification of the equation proposed in [10]:

$$\sigma = \sqrt{3}\left[a\varepsilon^{n}\exp\left(\frac{\beta}{T+273}\right)\exp(-q\varepsilon) + [1-\exp(-q\varepsilon)]a_{sat}\exp\left(\frac{\beta_{sat}}{T+273}\right)\right]\left(\sqrt{3}\dot{\varepsilon}\right)^{m} \tag{3}$$

where: ε – strain, $\dot{\varepsilon}$ – strain rate, T – temperature, °C,

There are 5 coefficients in equation (2) and 7 coefficients in equation (3). The values of these coefficients, determined using inverse analysis are given in **Table 2** for the steel 30CrMo12 and in **Table 3** for the steel 34CrNiMo6. Values of the objective function (1), which represent accuracy of the inverse analysis, are also given in these tables.

Figure 4 shows comparison of the loads measured in the tests and calculated by the FE program with the equation (2) implemented in the constitutive law. These plots show quite good capability of the function (2) to reproduce the real behaviour of the investigated steel 34CrNiMo6 in a wide

Table 2. Coefficients in equations (2) and (3) obtained from the inverse analysis for steel 30CrMo12.

Eq.	A	n	B	m	C			Φ
(2)	13525	0.28	0.59686	0.16204	4.089×10^{-3}			0.060434
Eq.	a	β	n	m	a_{sat}	β_{sat}	q	Φ
(3)	0.17455	7967.4	0.14186	0.16651	6.7686	716.28	0.33465	0.069176

Table 3. Coefficients in equations (2) and (3) obtained from the inverse analysis for steel 34CrNiMo6.

Eq.	A	n	B	m	C			Φ
(2)	7136.6	0. 172	0. 3693	0. 1718	3.7455×10^{-3}			0.05276
Eq.	a	β	n	m	a_{sat}	β_{sat}	q	Φ
(3)	0. 3411	7122.1	0. 1817	0. 1719	2.6077	6.7167	0. 4194	0.05115

range of temperatures and strain rates. Similar, very good agreement between measurements and predictions of loads was obtained for the second steel 30CrMo12, as well as for equation (3) for both steels, and these results are not shown here.

Finite Element Model. The developed rheological model was implemented in the FORGE finite element code, which was used for simulation of forging of crank shaft. The model applied in the Forge 3 FE code is based on the Norton-Hoff constitutive law [11, 12] and is described in [13]. This law is generally written in the form of relationship between stress tensor ($\underline{\boldsymbol{\sigma}}$) and the strain rate tensor ($\underline{\dot{\boldsymbol{\varepsilon}}}$):

$$\underline{\boldsymbol{\sigma}} = 2K\left(\sqrt{3}\dot{\varepsilon}_i\right)^{m-1}\underline{\dot{\boldsymbol{\varepsilon}}} \tag{4}$$

The value of $m = 1$ corresponds to the Newtonian fluid with a viscosity $\eta = K$, $m = 0$ is the plastic flow rule for a rigid-plastic material obeying the Levy-Mises flow rule and the Huber-Mises yield criterion. The value of $m = 0.16204$ is used in the present work and the relation between the yield stress and the constant K is:

$$K(T, \varepsilon, \dot{\varepsilon}) = \frac{\sigma}{\sqrt{3}^{m+1}\dot{\varepsilon}_i^m} \tag{5}$$

Yield stress σ in the Norton-Hoff model is described as a function of temperature, strain rate and strain using equations (2) or (3). Mechanical solution is coupled with the thermal model, which is based on the finite element solution of the Fourier equation.

Simulations

Modified TR process. The idea of the modified TR process is presented in **Figure 5** in the form of the FE model

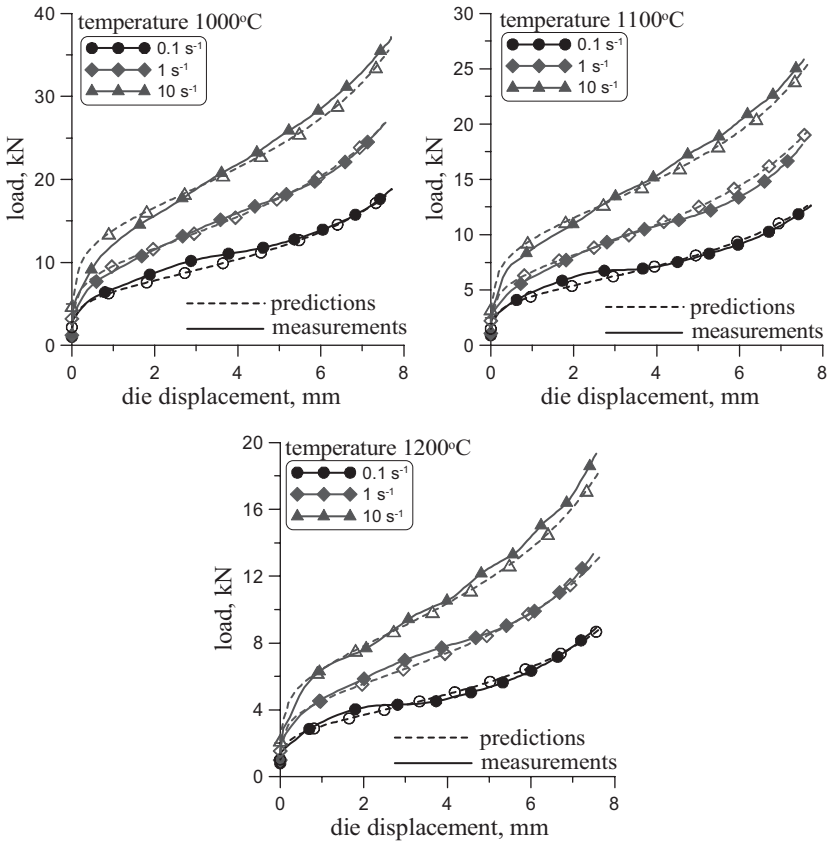

Figure 4. Comparison of measured loads with results of FE calculations using equation (2) with coefficients in Table 2 as rheological law, for the 34CrNiMo6 steel.

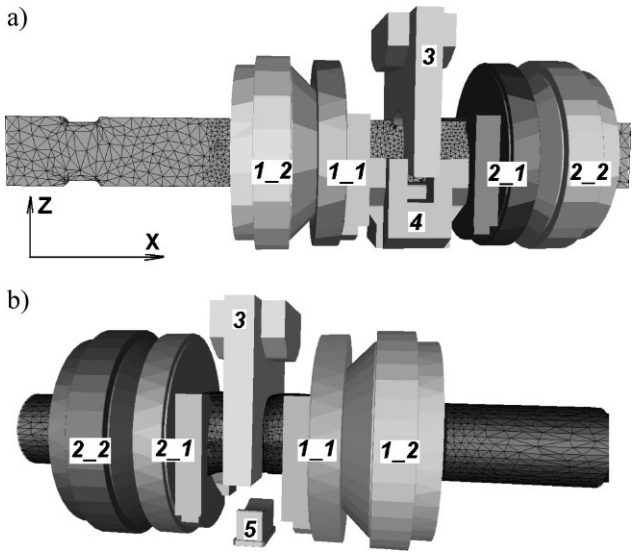

Figure 5. The process model (variant I) generated in Forge 3: (a) unsymmetrical pre upsetting b) forging of the crank throw.

[14, 15]. The sets of dies for unsymmetrical preupsetting, which distinguishes the considered process from the conventional one, is shown in Figure 5a. Beyond face die inserts (1_1; 2_1), clamping die inserts (1_2; 2_2), bending tool (3), one more additional tool – foreanvil (4) –, which bends the material to form the crank at this primary stage of the process, is also shown in this figure. The sets of dies for forging of the crank throw are shown in Figure 5b. The foreanvil (4) was replaced with anvil (5). The variant presented in Figure 5 is the main variant of the modified process (I) and the remaining variants are obtained by removing various tools.

Beyond variant I, in which all the tools are used, the following variants are considered:
II – Without the anvil (5).
III – Without the juts (3a) at both sides at the top of the bending tool (3). These juts form the shape of the top part of the crank webs in variants I and II.
IV – Without the anvil (5) and without the juts at both sides at the top of the bending tool (3).

The stock material (workpiece) with grooves is presented in **Figure 6**. Due to symmetry of the shape and boundary conditions, only half of the workpiece is considered in simulations. The finite element mesh with 60000 elements was generated. The number of elements was changing due to remeshing. The number of nodes was changing, as well, between 12000–15000. Friction factor 0.8 in Tresca model was assumed. Initial temperature was 1180 °C. As flow stress model the equation (2) was used for steel 30CrMo12. The set of tools for the first stage (unsymmetrical pre upsetting) in variant I is shown in **Figure 7**.

Results and analysis. The idea of the computer aided forming technology design proposed in [16] was applied. Simulations were performed for four variants of the forging technology. The analysis aimed at the forces acting on tools and the metal flow during forging. The following forces were considered:
F_{x1}, F_{x2} – forces acting on face die insert 1_1 and clamping die 1_2 in figure 5, along the axis of the workpiece (axis X).
F_{z3} – force acting on the bending tool, number 3 in Figure 5, perpendicular to the axis of the workpiece.
F_{z5} – force acting on the anvil, number 5 in Figure 5, perpendicular to the axis of the workpiece.

Figure 8 shows forces during preliminary upsetting acting along the axis of the workpiece (F_{x1}, F_{x2}) and force (F_{z3})

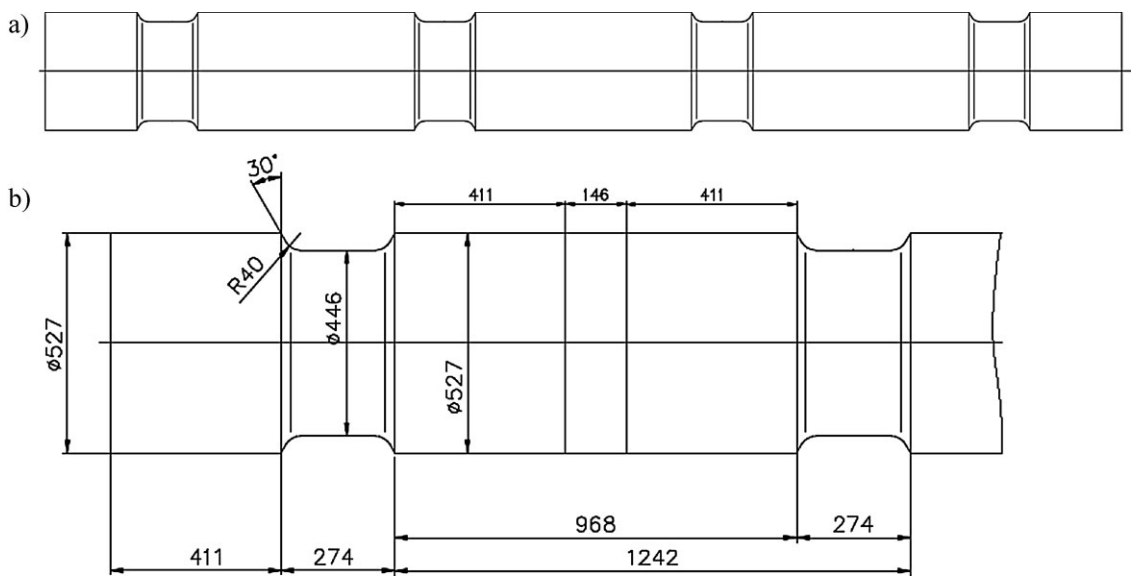

Figure 6. Shape (a) and dimensions (b) of the stock material.

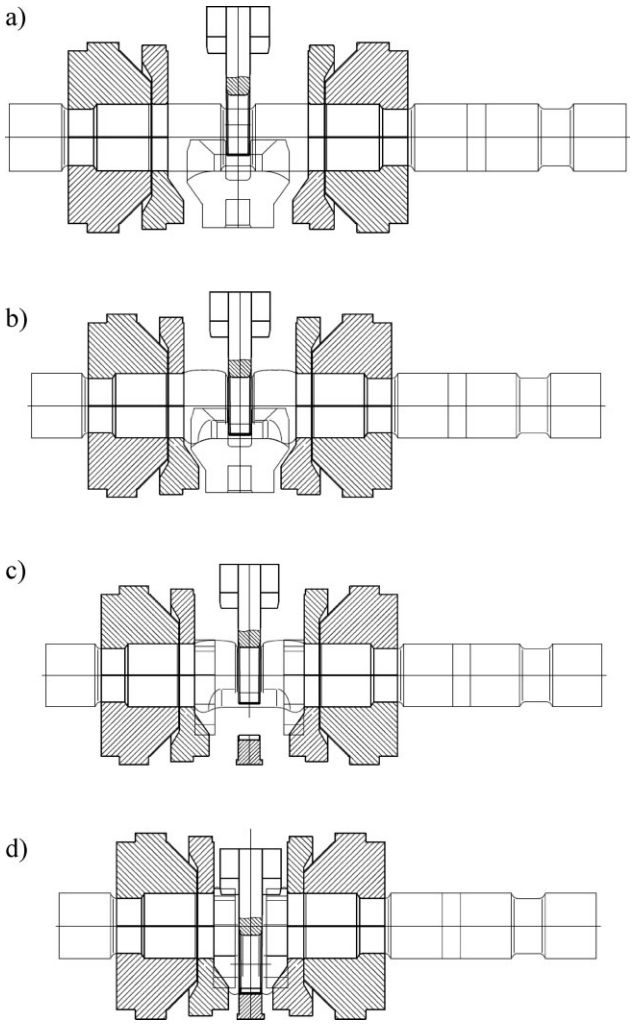

Figure 7. Schematic illustration of forging: a) beginning of the unsymmetrical preupsetting; b) end of the unsymmetrical preupsetting; c), beginning of the forging of the crank throw; d) end of the forging of the crank throw.

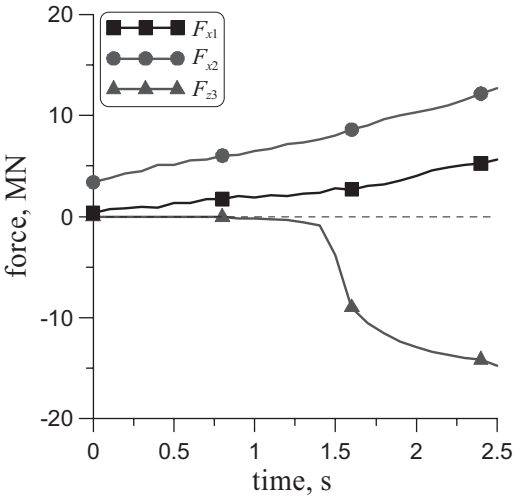

Figure 8. Forces during the unsymmetrical pre upsetting.

perpendicular to this axis acting on the bending tool (3), which forms the shape of the forging at the final stage of unsymmetrical pre upsetting, is also shown. Maximum force of pre upsetting is 17.3 MN ($F_{x1}+F_{x2}$). Maximum force acting on the bending tool (3) is 14.7 MN. Metal flow during unsymmetrical pre upsetting can be observed in **Figure 9**, where distribution of the displacement along the Z axis (U_z) is shown. The range of displacements along this axis is 23-26 mm in the direction opposite to the motion of the bending tool (3). The unsymmetrical pre upsetting process was identical for the four considered forging technologies.

Analysis of the crank forging stage was performed for four variants presented above. **Figure 10** shows a comparison of the forces acting on the tools in the considered variants. The largest constraint of material flow is observed in variant I. Maximum horizontal force at the final stage of the process is 48.2 MN ($F_{x1}+F_{x2}$). Force acting on the bending tool (3) (F_{z3} in Figure 10a) changes only slightly during the major part of the process. It begins to increase slowly when metal gets in contact with the tools 1_1 and 1_2. This increase becomes rapid when bending tool (3) begins to form the crank. It happens about 5.4 s before the end of the process, see F_{z5} in Figure 10a. The force acting on the bending tool reaches 33.6 MN. Removing of the anvil (5) (variant II) causes a situation, in which an increase of the load on the bending tool (3) is caused by the influence of the tools 1_1 and 1_2, see Figure 10b. In consequence, the total force in this variant is lower and the maximum values are in horizontal direction $F_{x1}+F_{x2}=43$ MN and in vertical direction $F_{z3}=25{,}2$ MN. Variant III differs from the variant I by the shape of the bending tool (3). The juts at both sides at the top of this tool are removed. Lack of these juts leads to slow increase of the force acting on the bending tool (3), until the contact between the journal and the anvil (5) begins, see curve for F_{z5} in Figure 10c. From that point this force increases rapidly and reaches 18.6 MN. Character of changes of the horizontal force is similar and its force reaches 41.8 MN. The last variant IV, which is performed without the anvil (5) and without the juts at both sides at the top of the bending tool (3), is characterized by the lowest

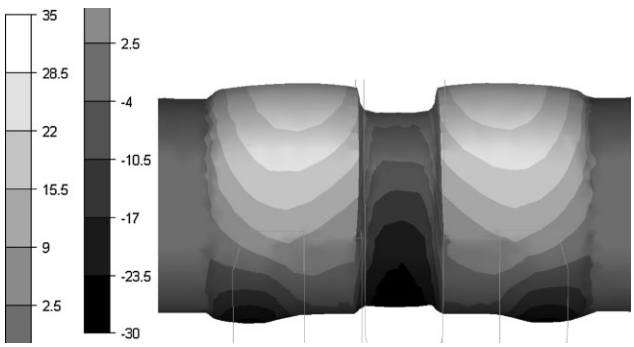

Figure 9. Distribution of the displacements U_z at the final stage of the unsymmetrical pre upsetting.

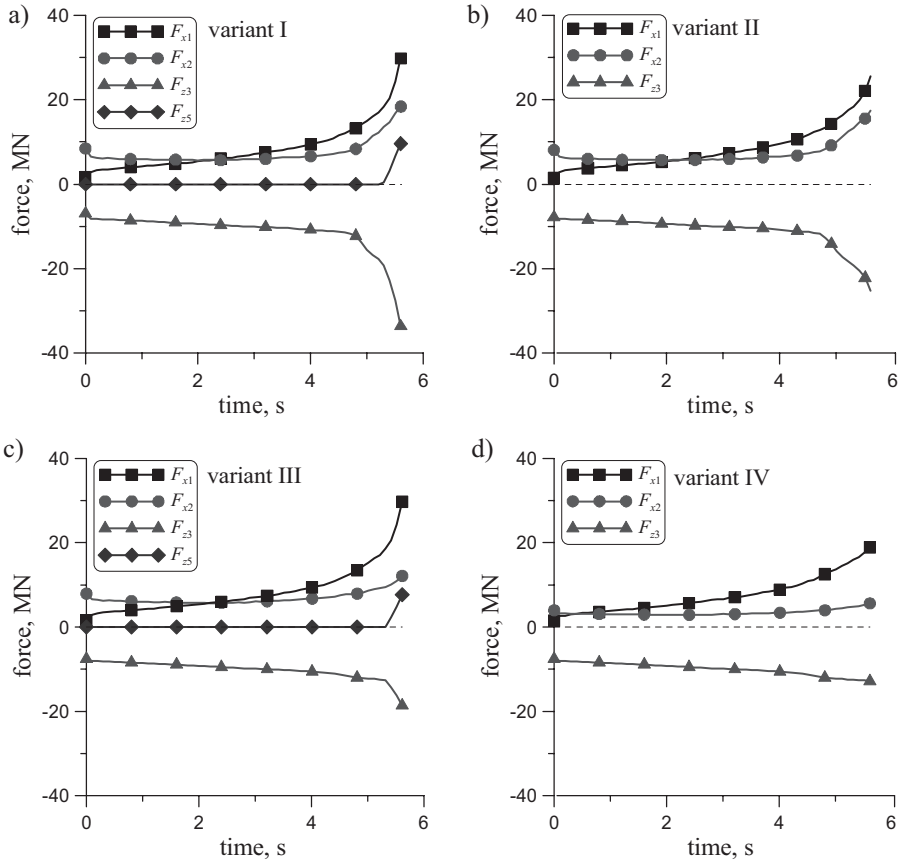

Figure 10. Forces acting on the tools in all considered variants: I – a, II – b, III – c and IV – d.

loads on all tools (Figure 10d). Horizontal force reaches 30.1 MN and vertical force acting on the bending tool reaches 12.9 MN. A shape of the crank obtained according to the four presented variants of technology is shown in **Figure 11**. Distribution of the displacement along the *Z* axis is show in this figure, as well.

The character of the metal flow in the central part of the crank web is similar for all variants. Due to the lack of the anvil in the variant II, thickening of the crank pin and decrease of the flash is observed. In the variant III, the top surface of the crank web is not shaped (free flow of the material). In consequence, more material is left in this top part and smaller flash is formed at the bottom die. Similarly to the variant III, in the variant IV the top surfaces of the crank web are not shaped. However, due to lack of the die, crank pin thickens and the flash is even smaller than in the variant III.

The obtained distributions of the temperature and deformation parameters make it possible to predict microstructure and phase composition of steel after forging. To reach this goal the results of research on phase transformations and microstructure of steels with similar chemical composition, performed in [17], should be used.

Conclusions

A concept for forging of crankshafts is presented in this paper. By introduction of additional tools efficient forging of crankshafts with more complicated shapes of crank webs is possible. The performed analysis confirmed that resistance to forming connected with forming of crank throws depends mainly of the degree of the constrain of the deformation zone. The largest resistance to deformation and, in consequence, the largest forces, are observed in variant I, in which all tools are used. The lowest loads were obtained in variant IV, in which two of the tools are eliminated. Loads in the variant I are approximately 70% larger than in the variant IV. Loads in variants II and III are comparable and they are about 30% larger than in the variant IV.

Having in mind the importance of accurate reproduction of the required shape of the crank throw, the application of the variant I is strongly recommended. In special cases only, when available load of the press is too small, one of the remaining variants can be used, but it may have destructive influence on the dimensional accuracy.

Beyond this, the analysis of results has show that loads necessary to form the crank throw depend strongly on the shape of crank webs of its crank throw. The more the shape is

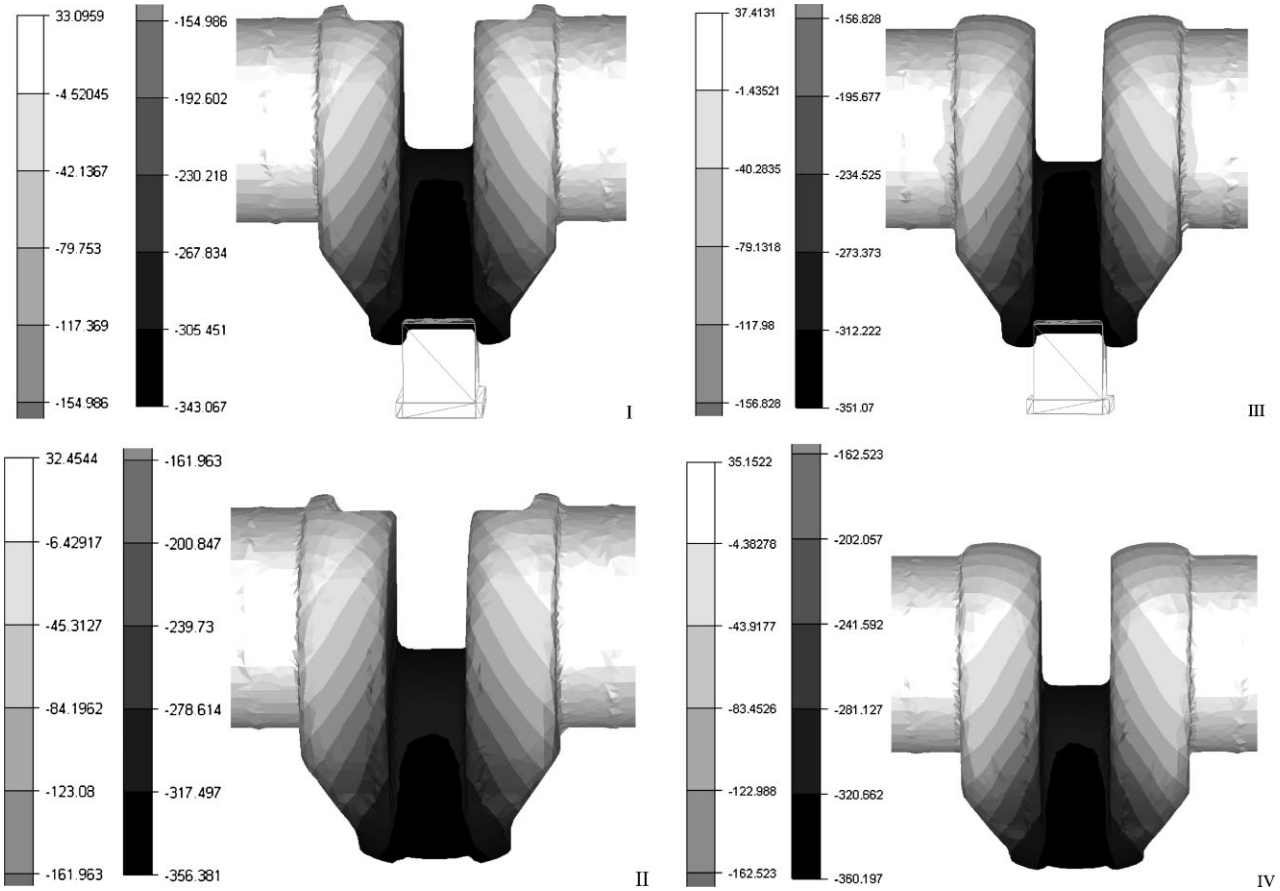

Figure 11. Distribution of the displacements U_z at the final stage of the forging, variant I, II, III and IV from the top.

close to an upside-down triangle or polygon, the larger are forming forces. This problem will be the topic of future work.

Acknowledgements

Financial assistance of the MNiSzW, project no. N 508 391 735, is acknowledged.

References

[1] T. Rut, W. Walczyk: Obróbka plastyczna Metali, vol. 11 (2000) pp. 5–8 (in Polish).
[2] T. Rut, W. Walczyk: Part I. Archiwum Technologii i Automatyzacji, Vol. 22 (2002) 177-186; Part II. Archiwum Technologii i Automatyzacji, Vol. 22 (2002) pp. 187–196 (in Polish).
[3] D. Szeliga, J. Gawąd, M. Pietrzyk: Comp. Meth. Appl. Mech. Engrg., Vol. 195 (2006) 6778–6798.
[4] B. Boyer, E. Massoni: Proc. 6th ICTP, Advanced Technology of Plasticity, ed., M. Geiger, Nuremberg, 1 (1999) pp. 347–352.
[5] R. Forestier, E. Massoni, Y. Chastel: J. Mat. Proc. Techn., Vol. 125 (2002) pp. 594–601.
[6] D. Szyndler, M. Pietrzyk, P. D. Hodgson: Proc. NUMIFORM, 2001, ed., K. Mori, Publ. A. Balkema, Toyohashi, 2001, 297–302.
[7] J. G. Lenard, M. Pietrzyk, L. Cser: Mathematical and Physical Simulation of the Properties of Hot Rolled Products, Elsevier, Amsterdam (1999).
[8] M. Pietrzyk: Finite Element Simulation of Large Plastic Deformation, J. Mat. Proc. Techn., 106, 2000, 223–229.
[9] A. Hansel, T. Spittel: Kraft- und Arbeitsbedarf Bildsamer Formgebungs-verfahren, VEB Deutscher Verlag fur Grundstoffindustrie, Leipzig (1979).
[10] A. Gavrus, E. Massoni, J.-L. Chenot: J. Mat. Proc. Techn., Vol. 60 (1996) pp. 447–454.
[11] F. H. Norton: Creep of Steel at High Temperature, McGraw Hill, New York (1929).
[12] N. J. Hoff: Quart., Appl. Mech., Vol. 2 (1954) 49.
[13] J.-L. Chenot, M. Bellet: in Numerical Modelling of Material Deformation Processes, (eds) P. Hartley, I. Pillinger, C. E. N. Sturges, Springer-Verlag, London, Berlin (1992) pp. 179–224.
[14] A. Milenin, W. Walczyk, M. Pietrzyk: Rudy Metale, 54 (2009) pp. 748–753 (in Polish).
[15] A. Milenin, W. Walczyk, M. Pietrzyk: Rudy Metale, Proc. Konferencja Sprawozdawcza Komitetu Metalurgii PAN, Krynica-Czarny Potok (2010) (in press).
[16] Ł. Rauch, Ł. Madej, S. Węglarczyk, M. Pietrzyk, R. Kuziak, Archives of Civil and Mechanical Engineering, 8, 2008, 157–165.
[17] F. Nurnberger, O. Grydin, M. Schaper, F. W. Bach, B. Koczurkiewicz, A. Milenin: Steel Research International 81(3), 2010, 204–209.

